

# Nematic Liquid-Crystal Necklace Structure Made by Microfluidics System

Yoshiko Takenaka,\* Miha Škarabot, and Igor Muševič



Cite This: *Langmuir* 2020, 36, 3234–3241



Read Online

ACCESS |



Metrics & More

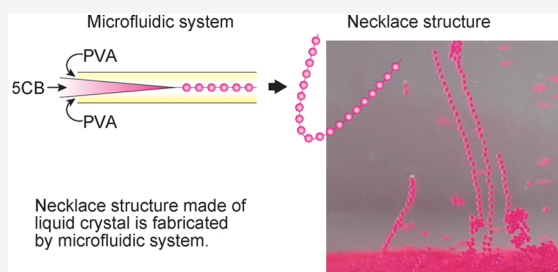


Article Recommendations



Supporting Information

**ABSTRACT:** We report a necklace structure made of liquid crystal dispersed in poly(vinyl alcohol) (PVA) aqueous solution, which is fabricated by a microfluidic device. In the necklace structure, liquid crystal droplets that are tens of micrometers in diameter are connected by microtethers, which are birefringent, are not penetrating the droplets, and can be elastically stretched by applying external force. The necklace structure was analyzed by fluorescent confocal microscopy, and the tethers were made of liquid crystal and PVA composite. The elastic constant of the tether was determined by using laser tweezers to stretch the tether. The Whispering Gallery Modes circulating inside individual droplets in the necklace structure were also observed.



## INTRODUCTION

Recently, many kinds of microstructures made of liquid crystals (LC) were studied for the applications in microlasers and optical microresonators: nematic droplets,<sup>1</sup> nematic shells,<sup>2</sup> cholesteric shells,<sup>3</sup> handle bodies,<sup>4</sup> fibers,<sup>5,6</sup> and liquid crystal drops threaded in cellulosic fibers.<sup>7–9</sup> In these necklace-like colloidal structures, individual LC microdroplets are threaded and thereby connected by microfibers, which become an impressive photonic superstructure. From the standpoint of light propagation, microspheres of high refractive index can support optical resonances that are known as Whispering Gallery Mode (WGM) resonances.<sup>10</sup> It has been demonstrated that WGM resonances in nematic liquid crystal droplets can be tuned by an external electric field,<sup>1</sup> which deforms the director structure and changes the phase condition for optical resonances. WGMs in nematic droplets are also very sensitive to the environment and can serve as autonomous microsensors with optical readouts.<sup>11</sup> Microfibers, which are connecting microspheres into the necklace-like structure, could in principle transport light between optical microresonators which is the main motivation for this work. This kind of a system of optically coupled microresonators is spontaneously formed which makes it an interesting photonic superstructure for potential application as a system of coupled optical sensors. In this study, we focus on the necklace structure made of a nematic liquid crystal.

Sometimes, the necklace structure is also called a spindle-knot structure.<sup>12–18,20–27</sup> This structure has been studied abundantly for the application in water collection, oil adsorption, and biomedical devices<sup>7–9,12–27</sup> because the structure is similar to that of spider silk. For instance, water vapor in the air adsorbs to the spindle parts of the spider silk and is gathered together at the knot parts to grow into a large

water droplet. The methods for the fabrication of the necklace structure have been reported previously and are based on electrospinning,<sup>13,14</sup> dip-coat method,<sup>7–9,15–17</sup> and microfluidics.<sup>18–27</sup> Some of the necklace structures reported in refs 7–9 are made of liquid crystal droplets, and others are made of polymer, paraffin, gas, and so forth.<sup>12–27</sup> In many of these methods, three components are necessary to produce the necklace-like structure.<sup>18–27</sup> In such cases, the necklace is made of two different components, and it is dispersed in the third component. Sometimes it can be taken out from the third component.<sup>19–21,25,27</sup> In the case of a dip-coat method, droplets are organized on the previously prepared tether.<sup>7–9,15–17</sup> In this case, only two components are necessary, and the procedure consists of two steps: the preparation of tethers and the organization of droplets on the tethers. It means that the necklace structure created by the dip-coat method has different components for the tether and the droplet, respectively.

Geng et al. fabricated the necklace structure made of liquid crystal droplets connected with the cellulose tether using the dip-coat method.<sup>7–9</sup> The alignment of liquid crystals inside the droplet and optical phenomena induced by the voltage application or temperature change was observed experimentally and analyzed theoretically. It has been demonstrated that the results are always affected by the interface between the

**Received:** January 14, 2020

**Revised:** March 5, 2020

**Published:** March 5, 2020

nematic liquid crystal and the tether made of cellulose. Defects exist inside the LC droplet due to the orientational anchoring of the liquid crystal on the fiber's surface.

In this study, we show the fabrication method and the structural details of the necklace structure. In the necklace structure, droplets of the nematic liquid crystal are connected to each other by tethers made of the LC and PVA composite without penetrating the droplets. This necklace structure can be fabricated by a one-step microfluidics method by using two components. The resulting necklace structure is stable against the liquid crystalline phase transition into the isotropic phase and against the change in the orientation of the liquid crystal molecules at the surface of the droplet, that is, from tangential to homeotropic (perpendicular) orientation. The structure is mechanically robust, and we can even transport it by using laser tweezers as well as elastically stretch the tether and measure the elastic constant of the tether.

## EXPERIMENTS

The methods of preparation of microfluidic devices are well-known, and we used the method inspired by Utada et al.<sup>28</sup> We have used the flow-focusing geometry (Figure 1) to fabricate large droplets (diameter  $>100\ \mu\text{m}$ ) and used the single coflow geometry (Figure 2) to produce smaller droplets (diameter  $<50\ \mu\text{m}$ ). From the two inlets of a microfluidic device, liquids for a dispersed phase and a continuous phase were driven by two syringe-pumps (World Precision Instruments AL-1002X, KF-Technology 1000). The dispersed phase was the nematic liquid crystal 4-cyano-4'-pentylbiphenyl (5CB; Tokyo Chemical Industry Co., Ltd.), and the continuous phase was the 5 wt % aqueous solution of poly(vinyl alcohol) 72000 (PVA; Merck).

In the case of necklaces with large droplets (Figure 1), the LC was injected through the tip with the  $70\ \mu\text{m}$  diameter and with the flow rate from 0.1 to  $16\ \mu\text{L}/\text{min}$ , whereas the PVA solution was injected in the outside capillary with the flow rate of  $1\text{--}160\ \mu\text{L}/\text{min}$ . The LC droplets are directed to additional capillary, and it is clear that LC droplets are connected with the thin tether (Figure 1b–d).

Necklaces with smaller droplets were created with the simple coflow geometry, where the LC droplets were created from the tips with 5 or  $3\ \mu\text{m}$  diameter and the PVA solution was flowing in the same direction in the outside capillary (Figure 2). The range of flow rates in both phases were the same as in the case of large droplets. We made an in situ observation of the spontaneous fabrication of the necklace structures by the transmission inverted polarization microscope and took photos and videos with a color camera (Canon EOS 550D) and with a high-speed B/W camera (Pixelink, PL-A741). The detailed fabrication method of a microfluidic device and technical details of experimental settings are described in Supporting Information.

After the necklace structure was generated in PVA 5 wt % aqueous solution in the microfluidic device, the dispersion was dropped on a glass slide and sandwiched by a cover glass with  $80\ \mu\text{m}$  spacers. The perimeter of the cover glass was sealed by a two-component epoxy glue (UHU PLUS). This sealed cell was used as a sample for the observation of necklaces under microscopes.

To measure the elastic constant of the tether connecting two neighboring droplets, we used two separate laser traps of infrared laser tweezers (Aresis Tweez 250Si). A separate laser trap grabbed each of the two droplets connected with the tether. The separation between the two traps was gradually increased, resulting in the straightening and then stretching of the flexible tether. The two traps were then stopped at a position where the maximal force was exerted from the traps to the droplets. Any further increase of the trap separation resulted in the release of the droplets from the trap due to the finite capturing force of the tweezers. In this position of maximal stretching of the tether, one of the traps was switched-off. The motion of the released droplet, driven by the force of the stretched tether, was then recorded, and the time dependence of the position of each droplet

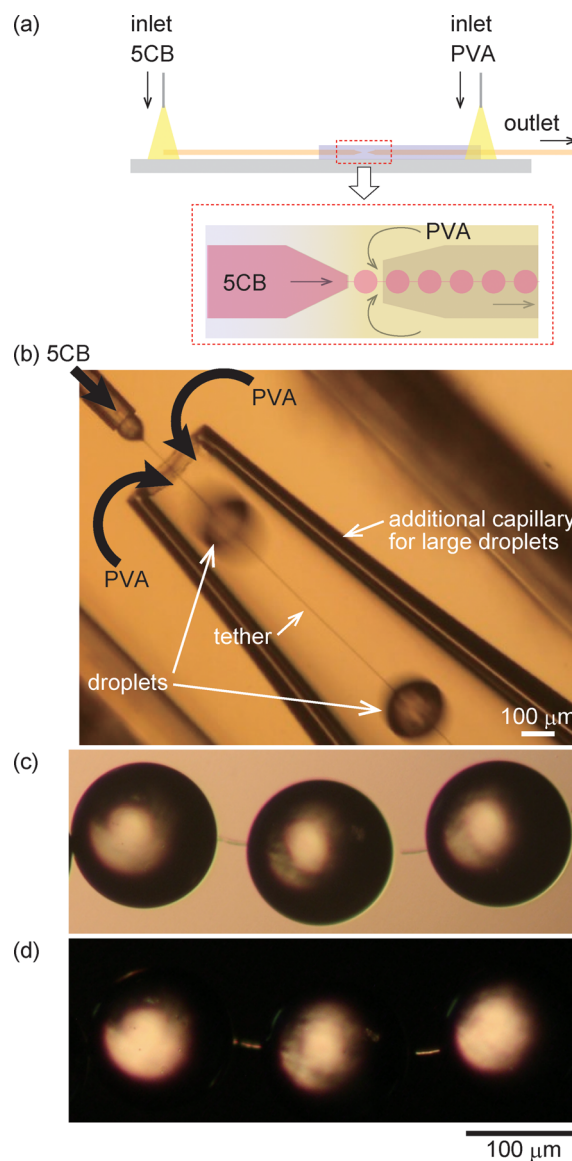


**Figure 1.** Formation of the necklace structure with large droplets (diameter  $>100\ \mu\text{m}$ ). (a) The schematic image of the microfluidic device of the flow-focusing geometry. (b) A snapshot of the necklace formation. (c) Nonpolarized optical microscopy image. (d) Crossed polarized microscopy image. The necklace structure was generated at a flow rate (5CB, PVA) = ( $5.0\ \mu\text{L}/\text{min}$ ,  $15\ \mu\text{L}/\text{min}$ ). The droplet diameter is  $135\ \mu\text{m}$ .

and their separation were analyzed by ImageJ software (Wayne Rasband, NIH). In overdamped motion, assuming the linear resilience of the tether, the elastic constant of the tether on the droplet was calculated from the calculated instantaneous velocity of the droplet and the viscosity of PVA 5 wt % aqueous solution measured by a rheometer (Anton Paar, Physica MCR 301).

An inverted polarization microscope (Nikon ECLIPSE TE-2000U) was used for the sample observation in transmission. In some experiments, a fluorescent confocal optical microscope (Leica TCS SP5 X) was used for detailed imaging of tethers in a system labeled with two different fluorescent dyes. The fluorescent mixture of 5CB and Nile Red (Sigma-Aldrich) was used instead of pure 5CB as described elsewhere,<sup>1</sup> and the fluorescent mixture of PVA and Fluorescein-5-isothiocyanate (FITC; Invitrogen) was used instead of pure PVA. The different dyes show different solubility in the liquid crystal and water, respectively. Nile Red is well dissolved in 5CB, but it does not mix with water. On the other hand, FITC dissolves well in

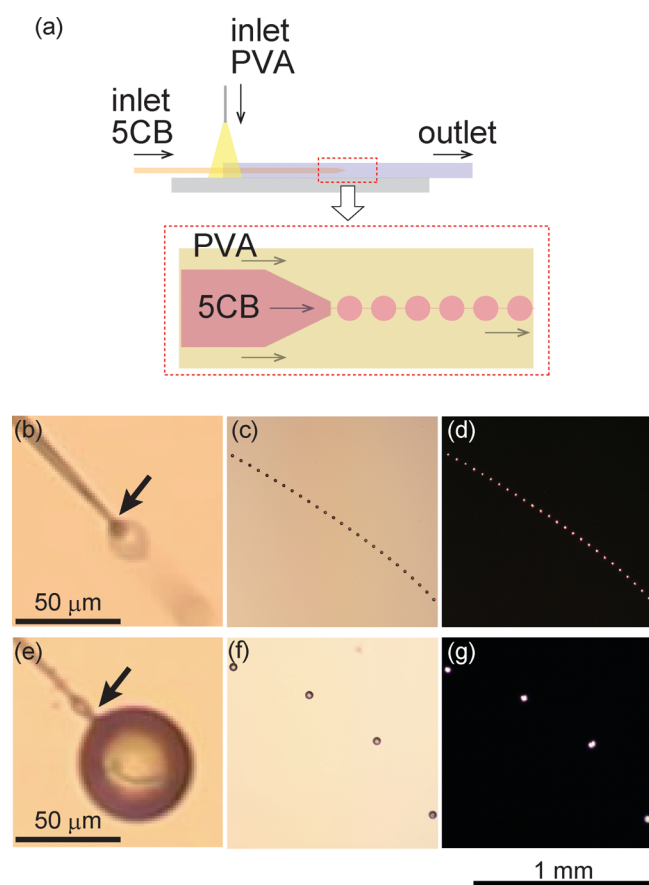


**Figure 2.** Formation of the necklace structure with small droplets (diameter  $<50 \mu\text{m}$ ). (a) The schematic image of the microfluidic device of the single coflow geometry. (b,e) Images of the tip, which is generating the droplets shown in (c,d) and (f,g), respectively. The images are snapshots taken from the videos; therefore, they are not as sharp. Each tip of the capillary is arrowed in each image. (c,f) Nonpolarized optical microscopy images of a necklace. (d,g) Crossed polarized microscopy images of a necklace. The scale bar of 1 mm is for these four images (c,d,f,g). The necklace structure was generated at a flow rate of (SCB, PVA) = (0.6  $\mu\text{L}/\text{min}$ , 36  $\mu\text{L}/\text{min}$ ) in images (c,d). The droplet diameter is 17  $\mu\text{m}$ . (f,g) Flow rate of (SCB, PVA) was (2.0  $\mu\text{L}/\text{min}$ , 90  $\mu\text{L}/\text{min}$ ), respectively. The droplets' diameter is 46  $\mu\text{m}$ .

water and does not mix with 5CB, which allowed for good fluorescent contrast between water-rich and liquid crystal-rich parts of the obtained confocal images.

The fluorescent mixture of 5CB and Nile Red fluorescent dye was also used for the inspection for WGM resonance of droplets connected with the tether. The dye inside the droplet was excited by the green Ar<sup>+</sup> laser (514.5 nm, Coherent Innova 90C), and the fluorescent light emitted from the droplet was analyzed by a spectrometer (Andor, SR-500L-D1).

## RESULTS AND DISCUSSION

The necklace structures can be generated within a specific range of experimental parameters, such as flow rate and PVA concentration. The flow rate of liquid crystal ranged from 0.1 to 16  $\mu\text{L}/\text{min}$ , and that of PVA aqueous solution ranged from 1 to 160  $\mu\text{L}/\text{min}$ . When the order of the flow rate is changed drastically, the necklace generation stops, and the laminar flow or a separated large droplet with low frequency is generated. For example, when the flow rate of the continuous phase was changed from 160 to 16  $\mu\text{L}/\text{min}$  and the flow rate of the

dispersed phase was fixed, the droplet size increased from 45 to 175  $\mu\text{m}$ , the generation frequency of droplets decreased from 90 to 5 Hz, and the necklace was not formed.

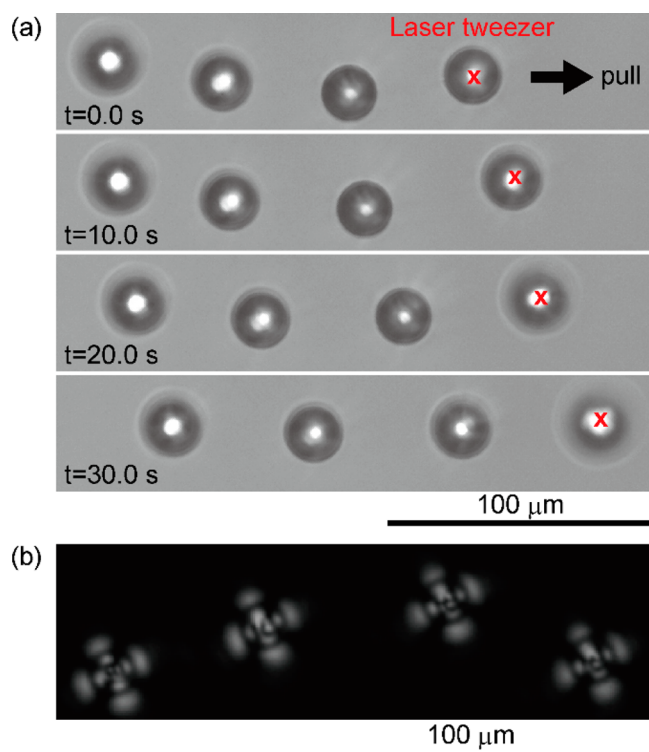
We used the flow-focusing geometry for large droplets (diameter  $>100 \mu\text{m}$ ) and the single coflow geometry for small droplets (diameter  $<50 \mu\text{m}$ ). A necklace structure was well generated in both geometries. The concentration of PVA aqueous solution for all experiments in this paper was 5 wt %. We did not optimize the concentration of the PVA solution, but the necklace structure was not generated with the 3 wt % PVA aqueous solution. If the concentration of the PVA aqueous solution becomes higher than 5 wt %, it will be more difficult to flow out because of the higher viscosity. We also experimented with oleic acid that does not mix with water instead of 5CB to check the importance of 5CB for the necklace formation. In the case of oleic acid and PVA aqueous solution, we could not make a necklace structure. This indicates that the physical properties of both the PVA aqueous solution and the liquid crystalline state of 5CB are essential for the generation of a necklace structure.

Figure 1 shows the generation of large liquid crystal droplets (diameter  $>100 \mu\text{m}$ ) connected with the tether. The process of generating the necklace structure is shown in Video 1. In this image, the tether is thick enough to be seen by optical microscopy. Details of the necklace structures are shown in Figure 1c,d. From the polarized microscopy images, we concluded that the nematic liquid crystal 5CB in the droplet shows the tangential alignment of the director at the surface of the droplet. This is expected because droplets are dispersed in the PVA solution, which usually induces the tangential alignment of the director at the interface (Figure 1d). In addition, the tether is also birefringent, because it appears bright between crossed polarizers in Figure 1d. Henceforth, the tether also contains orientationally ordered LC.

Figure 2 shows the generation of small liquid crystal droplets (diameter  $<50 \mu\text{m}$ ) connected with the tether. The process of generating the necklace structure is shown in Video 2 and Video 3. Figure 2 also shows the tips generating each droplet. Previous studies showed that the size of droplets depends on the tip structure (such as type and dimension), fluid properties (such as density, viscosity, surface tension, and wall contact angle), and operating parameters (such as pressure, flow rate ratio, and average velocity).<sup>29,30</sup> In our experiments, the size of droplets varies from about 15  $\mu\text{m}$  to about 250  $\mu\text{m}$  depending on the tip diameter. Two such examples are presented in Figure 2.

The thickness of the tether is about 1  $\mu\text{m}$  for the 150  $\mu\text{m}$  droplets, whereas in the case of smaller droplets the tether is too thin to be seen by the optical microscopy. The flow rates can control the length of the tether. When the flow rate of 5CB increases or when the flow rate of PVA decreases, the length of the tether decreases. Although the droplets in Figure 2c,f seem to be disconnected from each other, this is not the case. We use laser tweezers to move them collectively by grabbing a single droplet only. It is a clear proof of a mechanical connection even though we cannot see the tethers due to their small diameter.

Although the laser tweezer could move all generated structures, it is easier to move smaller necklace structures due to a finite grabbing optical force of the tweezers. Figure 3 shows snapshots of the motion of the small necklace structure pulled by the laser tweezer. (The process of moving the necklace with tweezers is shown in Video 4.) The droplet



**Figure 3.** (a) Snapshots of the motion of the small necklace structure that is pulled by the laser tweezer. The red cross indicates the position of the laser trap, which is moving to the right. The images were picked up from the Video 4. (b) The necklace structure of 5CB droplets with homeotropic (perpendicular) alignment. This image is taken between crossed polarizers.

could clearly follow the motion of the optical trap of laser tweezers. The distance between two droplets at first increases, but after the tether is stretched it becomes constant.

We should stress that all necklace structures could be produced in the PVA–water environment, which itself provides parallel anchoring of 5CB molecules at the surface of the LC droplet. However, once the necklace was formed, the molecular alignment of liquid crystals inside the droplet could be changed from parallel to homeotropic alignment by adding a surfactant that changes the surface alignment of 5CB from parallel to perpendicular. This was done by adding 0.1 mM cetyltrimethylammonium bromide (CTAB; Sigma-Aldrich) aqueous solution to the same amount of necklace dispersion in PVA solution. By this procedure, the director structure inside the droplet was changed from bipolar to radial. The radial structure can easily be recognized from images of droplets between crossed polarizer, shown in Figure 3b. The tether was preserved after the addition of the CTAB surfactant, which was proven by moving the necklace structure of radial nematic droplets using the laser tweezer (Video 5).

The tether is also stable against an increase in temperature beyond the nematic–isotropic phase transition temperature. We changed the phase of liquid crystal in the droplet from nematic to isotropic by increasing the laser power to increase the temperature. Because of the absorption of light, the liquid crystal is locally heated. At the higher power of the laser tweezers, the liquid crystal near the laser trap melts from the nematic to the isotropic phase. When the liquid crystal is in the isotropic phase, the birefringence of the liquid crystal vanishes, and the field of view is completely dark. Following the decrease

in temperature by decreasing the laser power, the droplets returned to the nematic phase and could again be seen by the polarized microscopy. This necklace structure could again be pulled by the laser tweezer (Video 6), which means that the tether was not cut by the phase transition and clearly indicates it does not consist of liquid crystal only.

To investigate the composition in the tether, we constructed the necklace structure made of the mixture of 5CB and Nile Red in the mixture of PVA solution and FITC. We observed this necklace structure by confocal microscopy (Figure 4a–d).

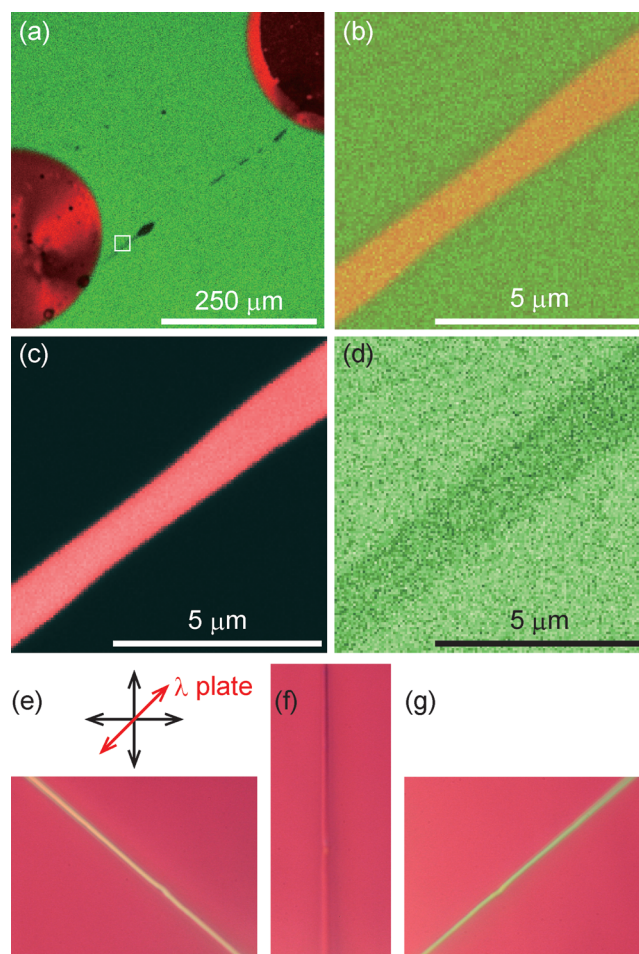


**Figure 4.** Details of the tether's structure. (a–d) Confocal microscopy images. The white squared region in (a) was enlarged to (b–d). The objective we used was 60 oil (NA 1.4). It means that the  $z$ -resolution is  $\sim 0.6 \mu\text{m}$ , and we looked at a very thin slice of a sample on panels b–d. (b) The combined image of Nile Red (red) and FITC (green). (c) The Nile-Red-rich part is enhanced in red color. (d) The FITC-rich part is enhanced in green color. (e–g) Observation with a  $\lambda$ -plate; (e) yellow shade, (f) red color, and (g) blue shade. The thickness of the tether is about  $1 \mu\text{m}$ .

The light for excitation is passed through an acousto-optic transmission filter (AOTF) that selects a narrow band of wavelengths from the continuous spectrum, typically 1–2 nm wide. Up to eight bands of excitation light can be selected at the same time by the AOTF. By selecting the proper wavelengths, we can observe the signal from the Nile Red and the FITC. The Nile Red image (Figure 4c) shows that 5CB is homogeneously distributed in the tether, and the FITC image (Figure 4d) shows that PVA is also distributed in the

tether like SCB. From these results, we can conclude that the tether is a stable composition of PVA and SCB. We have shown that the necklace structure was broken neither by the change in the alignment of liquid crystal in a droplet nor by the phase transition of the liquid crystal in a droplet. These results are reasonable because PVA, which occupies part of the tether, is not influenced either by the addition of CTAB that induces the change in the alignment of liquid crystal in a droplet nor the temperature change, which induces the phase transition of the liquid crystal in a droplet.

In order to reveal the molecular alignment in the tether, the inner structure of a larger diameter tether was observed by using the full-wave retardation ( $\lambda$ , red) plate (Figure 4e–g). This technique allows for the determination of the local orientation of the optical axis in liquid crystals<sup>31</sup> and hence the orientation of LC molecules. One can see from Figure 4e–g that the color of the tether in images with the red plate changes from yellow to red and blue when the tether is rotated with respect to the direction of the red plate's axis. These results clearly show that the tethers are made of birefringent material with the optical axis aligned along the length of the tether. The birefringence is induced by SCB, which is aligned to the direction of the tether because the refractive index anisotropy of SCB is positive. Additionally, some birefringence could also be induced by the PVA, which probably flow-aligns parallel to the tether during the flow of the material through the nozzle of the microfluidic capillary. It is interesting to note that although the LC orientation in the tether cannot be modified by changing the LC orientation in the droplet or by changing the temperature, we have observed long-term changes in the tethers. In some necklaces, LC and PVA in the tether segregated after some time, forming "pockets" of one phase in another. (See Supporting Information, Figure S1.)

To get insight into the mechanical properties of the tethers, we have stretched the tether with the laser tweezers and determined elastic properties of the tether. By using two optical traps, we trapped two adjacent droplets placed at the end of the necklace. The first trap fixed the droplet far from the end, and the other droplet was pulled by the second trap to stretch the tether. The tether was stretched to the maximal possible elongation (around  $\sim 1.5 \mu\text{m}$ ), and the droplet was released. We observed that the released droplet was returning slowly to the original position due to the tension of the tether (Video 7), indicating elastic deformation of the tether and absence of any hysteresis. The time dependence of the separation between two droplets, which is equal to the length of the tether, is shown in Figure 5. In this case, the stress-free length of the tether, that is, the stress-free distance between two droplets, is  $39.3 \mu\text{m}$ . This length is determined by the flow rates in the generation of the necklace structure.

Because of the small Reynolds number,  $\text{Re} \sim 10^{-7}$ , the acceleration of the droplet is negligible during the movement exerted by the tether. It follows that the force of the tether on the droplet is at all times equal to the viscous drag force

$$\vec{F}_{\text{tether}} + \vec{F}_{\text{viscosity}} \approx 0 \quad (1)$$

By using the Stokes law, we obtain the relation between the elastic force of the tether and the velocity of the droplet

$$F_{\text{tether}} = -F_{\text{viscosity}} = -6\pi R\eta \frac{dx}{dt} \quad (2)$$

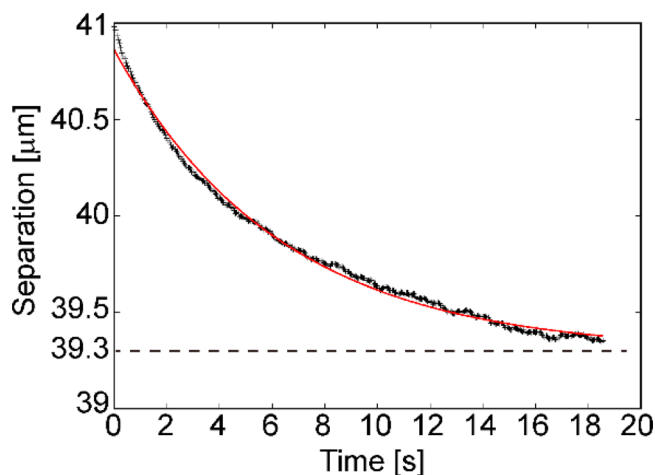


**Figure 5.** Time dependence of the separation between the two droplets when they are released from the trap of the tweezers and approach each other. The separation as a function of time was fitted by the exponentially decaying function of time  $f(t) = x_0 e^{-bt} + L$  with  $b = 0.16 \text{ s}^{-1}$ . The dotted line is the natural length of a tether obtained from the fitting.

Here the radius  $R$  of the droplet is measured under the microscope, and the viscosity  $\eta$  of the PVA aqueous solution was measured in a separate experiment:  $\eta \approx 59 \text{ mPa}\cdot\text{s}$  (see details in Supporting Information). Assuming the linear resilience of the tether for the small displacement, that is, Hook's law  $F_{\text{tether}} = kx$ , and solving the differential equation, we obtain the following time dependence of the elongation  $x$

$$x = x_0 e^{-kt/6\pi R\eta} \quad (3)$$

where  $x_0$  is the initial elongation of the tether. From this equation, we can obtain the time dependence of the separation between two droplets  $f(t)$  as

$$f(t) = x_0 e^{-kt/6\pi R\eta} + L \quad (4)$$

where  $L$  is the natural length of the tether. By fitting the data in Figure 5 with exponentially decaying function using gnuplot (Thomas Williams, Colin Kelley), we can determine the spring constant of the tether that is, in this case,  $k \approx 1.6 \mu\text{N}/\text{m}$ .

The Young's modulus  $E$  of the tether can be calculated from the spring constant  $k$ , length  $L$ , and cross-section  $S$  of a tether as  $E = kL/S$ . Whereas we can measure the natural length  $L$  quite accurately using the optical microscope, the diameter of the tether is too thin to be measured optically. We, therefore, made a very rough assumption that the diameter of the tether is linearly proportional to the diameter of the droplet to get estimated tether's diameter of  $\sim 100 \text{ nm}$  for  $20 \mu\text{m}$  droplet. Then, we obtain the rough approximation of tether's elastic modulus  $E \cong 8 \text{ kPa}$ . This is quite low compared to Young's modulus of electrospun PVA fiber, which is several GPa but is comparable to that of a PVA hydrogel, which is several tens of kPa.<sup>32</sup> Therefore, Young's modulus of the SCB/PVA tether obtained in this study is similar to that of a PVA hydrogel.

After all the experimental evidence is considered, it is clearly seen that the tether, connecting SCB droplets into the necklace structure, is made of an elastic composite similar to PVA hydrogel, which clearly contains orientationally ordered nematic LC SCB. The liquid crystal is ordered along the tether and contributes most of the birefringence to the structure.

We do not have clear evidence on the mechanism that is responsible for the formation of tethers, but we can conjecture that it originates from the strong orientational interactions between LC and PVA molecules. PVA is well-known to impose strong orientational anchoring of LC molecules and was used a long time ago as a surface alignment layer in LCDs. It is clear from our analysis of tethers that they contain LC that can only come from droplets. Evidently, LC molecules are pulled from the water–LC interface by the flowing PVA molecules due to their strong orientational (and likely positional) interaction, resulting in continuous desorption of the LC from the surface into the flowing PVA, which leads to the formation of a composite of LC and PVA that does not mix with water anymore. Furthermore, necklaces were formed in the dripping microfluidic regime, where both Capillary and Weber numbers are smaller than unity. It follows that surface tension forces between PVA and LC prevail over viscous shear stress force and inertial forces of LC. The calculation of Capillary and Weber numbers is presented in the [Supporting Information](#).

Finally, we were curious whether we could observe WGM in droplets and also the transport of light through the tether connecting two adjacent droplets. The existence of WGMs in droplets connected with tethers is not a trivial question because we do not know whether the tether perturbs the curved surface of the droplet to the level where the optical quality of the droplet cannot sustain any more WGMs. The SCB liquid crystal was doped with a small amount of Nile Red fluorescent dye, which is standard procedure when WGMs are studied in liquid crystal microresonators.<sup>1</sup> The necklace structure made of the mixture of SCB and Nile Red in PVA was used for experiments. The edge of the selected droplet was irradiated by a green line of the Ar<sup>+</sup> laser, and we have observed a characteristic picture of WGM, presented in [Figure 6b](#). One can clearly observe the fluorescent region on the opposite side of the droplet, which indicates that light is circulating in the interior of the droplet by a series of total internal reflections at the SCB–water interface. When the optical path for one circulation of this light is equal to half of an integer of the wavelength, the condition for the WGM optical resonance is fulfilled. We collected the light from the squared region of the droplet in [Figure 6b](#) and analyzed its spectrum with the spectrometer. [Figure 6c](#) shows the spectrum of fluorescent light, which is a typical WGM spectrum. The separation between the different WGM lines is small because the droplet is big, and the resonance condition is fulfilled for very large integer numbers. The WGM peaks are rather broad, indicating a rather low *Q*-factor of this microresonator. Low *Q*-factor can be attributed to several possible origins. First, light losses due to fluorescent emission from fluorescent dye could be significant. Second, the curved surface could be perturbed by the tether, penetrating the surface of the droplet. Third, defects are ubiquitous in these droplets, which strongly scatter light and reduce the *Q*-factor.

We tried to observe the transport of this WGM light through the tethers between adjacent droplets, but the experiments were negative, and no light could be seen being guided through the tethers. There are two possible reasons for the insufficient coupling of WGM light into the tether. First, the diameter of the tether ( $\sim 1 \mu\text{m}$ ) is most likely too small to sustain the optical modes in such a tiny optical waveguide. In future work, we should find a way to increase the thickness of the tether for possible optical applications. Second, the WGM light cannot couple efficiently into the tether because of the geometry of the

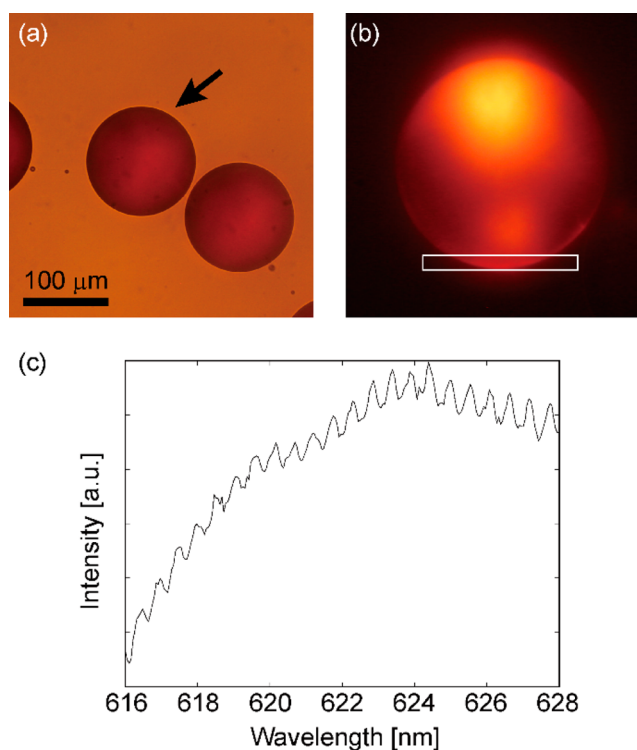


**Figure 6.** Observation of WGMs in SCB bipolar droplets. (a) Microscopy image of SCB droplets in PVA aqueous solution. The arrowed droplet is enlarged in (b). (b) Image of the droplet excited by a green laser. The light was collected from the white squared region, and the spectrum of this light was analyzed by the spectrophotometer. (c) Characteristic WGM spectrum of light, emitted from the fluorescently labeled SCB droplets is observed.

droplet-tether junction. Namely, WGMs can be considered as light circulating inside the droplet by subsequent total internal reflection. Because of a small difference between the refractive indices of LC ( $n = 1.5$ ) and water ( $n = 1.33$ ), the light is bouncing off the surface at very large angles (measured from the surface normal), since the angle of total reflection for the LC–water interface is  $\sim 62^\circ$ . With such a large angle, the WGM light enters into a tether at very small angle (measured from the normal to the interface), which is well above the angle of total reflection for the tether–water interface. This means that all WGM light will leak out at the junction. A solution to this coupling problem is to use another type of droplet, which is made of chiral nematic liquid crystal (CNLC) with parallel surface anchoring of LC at the surface of the droplet. Such a droplet presents an onion-Bragg optical microcavity, where the CNLC makes a series of concentric shells, wrapped one after another. It was demonstrated that such a droplet emits light in all directions which means that the direction of laser emission is perpendicular everywhere to the surface of the droplet.<sup>33</sup> If so, light emitted from the CNLC droplet will enter into the tether practically along the axis of the tether and will be strongly guided by the tether. However, this experiment is well beyond the scope of this article and will be presented elsewhere.

## CONCLUSIONS

Liquid crystal necklace can be made with a one-step process by injecting SCB into the PVA water solution through a microfluidic device. Diameters of the droplets and the tethers

can be tuned by the diameter of the capillary's tip for the dispersed phase and by the flow rates of dispersed and continuous phases. The droplet part of a necklace structure consists of 5CB and the tether part is a gel-like composite of both 5CB and PVA. The necklace structure is mechanically stable against the changes in the phase and the surface alignment of the 5CB. In addition, the structure is robust, can be pulled by tweezers, and can be kept for at least three months in PVA 5 wt % solution. The necklace structure made of liquid crystal and PVA shows WGMs and has exciting potential for the application in optical devices, especially for a system of mutually connected 3D microlasers made of chiral nematic liquid crystals.

## ■ ASSOCIATED CONTENT

### Supporting Information

The Supporting Information is available free of charge at <https://pubs.acs.org/doi/10.1021/acs.langmuir.0c00101>.

Fabrication of a microfluidic device; experimental setting of a microfluidic device; calculation of the Capillary and Weber numbers; segregation of a liquid crystal in a tether; measurement of the viscosity of a PVA solution; additional references (PDF)

Video 1 of process of generating necklace structure (diameter  $\sim 135 \mu\text{m}$ ) (MP4)

Video 2 of process of generating necklace structure (diameter  $\sim 17 \mu\text{m}$ ) (MP4)

Video 3 of process of generating necklace structure (diameter  $\sim 46 \mu\text{m}$ ) (MP4)

Video 4 of process of moving necklace with tweezers (AVI)

Video 5 of process of moving necklace structure of radial nematic droplets using laser tweezer (MP4)

Video 6 of process of moving necklace structure with nematic–isotropic transition pulled by the laser tweezer (AVI)

Video 7 of stretched and released droplet returning slowly to original position due to tension of tether (AVI)

## ■ AUTHOR INFORMATION

### Corresponding Author

Yoshiko Takenaka – Research Institute for Sustainable Chemistry, National Institute of Advanced Industrial Science and Technology (AIST), Tsukuba, Ibaraki 305-8565, Japan; [orcid.org/0000-0001-9587-5720](https://orcid.org/0000-0001-9587-5720); Email: [takenaka.yoshiko@aist.go.jp](mailto:takenaka.yoshiko@aist.go.jp)

### Authors

Miha Škarabot – Jožef Stefan Institute, 1000 Ljubljana, Slovenia

Igor Muševič – Jožef Stefan Institute, 1000 Ljubljana, Slovenia; Faculty of Mathematics and Physics, University of Ljubljana, 1000 Ljubljana, Slovenia

Complete contact information is available at:

<https://pubs.acs.org/doi/10.1021/acs.langmuir.0c00101>

### Author Contributions

All authors contributed equally to this manuscript. All authors have approved the final version of the manuscript.

### Notes

The authors declare no competing financial interest.

## ■ ACKNOWLEDGMENTS

This study was done by fundamental research funds of Jožef Stefan Institute in Slovenia and AIST in Japan. The authors thank Dr. Yoshiaki Uchida and Ms. Eriko Moriwaki (Osaka University, Japan) for their support in fabrication of microfluidic devices, Dr. Uroš Tkalec (Jožef Stefan Institute, Slovenia), Mr. Rok Štanc (Maribor University, Slovenia), and Dr. Masamune Morita (AIST, Japan) for their support in the of the capillary, Prof. V. S. R. Jampani (University of Luxembourg, Luxembourg) for providing the data on surface tension, Dr. Maruša Mur (Jožef Stefan Institute, Slovenia) for her experimental help with confocal microscopy, Dr. Hiroyuki Kitahata (Chiba University, Japan) for his help for the analysis of elastic constant of a tether, and Prof. Danjela Kušcer (Jožef Stefan Institute, Slovenia) for her experimental help in the measurement of the viscosity of the PVA solution.

## ■ REFERENCES

- (1) Humar, M.; Ravnik, M.; Pajk, S.; Muševič, I. Electrically tunable liquid crystal optical microresonators. *Nat. Photonics* **2009**, *3*, 595–600.
- (2) Lopez-Leon, T.; Koning, V.; Devaiah, K. B. S.; Vitelli, V.; Fernandez-Nieves, A. Frustrated nematic order in spherical geometries. *Nat. Phys.* **2011**, *7*, 391–394.
- (3) Uchida, Y.; Takanishi, Y.; Yamamoto, J. Controlled Fabrication and Photonic Structure of Cholesteric Liquid Crystalline Shells. *Adv. Mater.* **2013**, *25*, 3234–3237.
- (4) Senyuk, B.; Liu, Q.; He, S.; Kamien, R. D.; Kusner, R. B.; Lubensky, T. C.; Smalyukh, I. I. Topological colloids. *Nature* **2013**, *493*, 200–205.
- (5) Toquer, G.; Phou, T.; Monge, S.; Grimaldi, A.; Nobili, M.; Blanc, C. Colloidal Shape Controlled by Molecular Adsorption at Liquid Crystal Interfaces. *J. Phys. Chem. B* **2008**, *112*, 4157–4160.
- (6) Peddireddy, K.; Jampani, V. S. R.; Thutupalli, S.; Herminghaus, S.; Bahr, C.; Muševič, I. Lasing and waveguiding in smectic A liquid crystal optical fibers. *Opt. Express* **2013**, *21*, 30233–30242.
- (7) Geng, Y.; Almeida, P. L.; Figueirinhas, J. L.; Terentjev, E. M.; Godinho, M. H. Liquid crystal beads constrained on thin cellulosic fibers: electric field induced microrotors and N–I transition. *Soft Matter* **2012**, *8*, 3634–3640.
- (8) Geng, Y.; Sec, D.; Almeida, P. L.; Lavrentovich, O. D.; Zumer, S.; Godinho, M. H. Liquid crystal necklaces: cholesteric drops threaded by thin cellulose fibres. *Soft Matter* **2013**, *9*, 7928–7933.
- (9) Terentjev, E. Interplay of topologies. *Nat. Mater.* **2013**, *12*, 187–189.
- (10) Ashkin, A.; Dziedzic, J. M. Observation of optical resonances of dielectric spheres by light scattering. *Appl. Opt.* **1981**, *20*, 1803–1814.
- (11) Humar, M.; Muševič, I. Surfactant sensing based on whispering-gallery-mode lasing in liquid-crystal microdroplets. *Opt. Express* **2011**, *19*, 19836–19844.
- (12) Zhu, H.; Guo, Z.; Liu, W. Biomimetic water-collecting materials inspired by nature. *Chem. Commun.* **2016**, *52*, 3863–3879.
- (13) Dong, H.; Wang, N.; Wang, L.; Bai, H.; Wu, J.; Zheng, Y.; Zhao, Y.; Jiang, L. Bioinspired Electrospun Knotted Microfibers for Fog Harvesting. *ChemPhysChem* **2012**, *13*, 1153–1156.
- (14) Du, M.; Zhao, Y.; Tian, Y.; Li, K.; Jiang, L. Electrospun Multiscale Structured Membrane for Efficient Water Collection and Directional Transport. *Small* **2016**, *12*, 1000–1005.
- (15) Bai, H.; Ju, J.; Sun, R.; Chen, Y.; Zheng, Y.; Jiang, L. Controlled Fabrication and Water Collection Ability of Bioinspired Artificial Spider Silks. *Adv. Mater.* **2011**, *23*, 3708–3711.
- (16) Dong, H.; Zheng, Y.; Wang, N.; Bai, H.; Wang, L.; Wu, J.; Zhao, Y.; Jiang, L. Highly Efficient Fog Collection Unit by Integrating Artificial Spider Silks. *Adv. Mater. Interfaces* **2016**, *3*, 1500831.
- (17) Lin, C. B.; Huang, Z.-H.; Liu, C.-Y. Formation of high-quality photonic nanojets by decorating spider silk. *Opt. Lett.* **2019**, *44*, 667–670.

- (18) Kang, E.; Jeong, G. S.; Choi, Y. Y.; Lee, K. H.; Khademhosseini, A.; Lee, S.-H. Digitally tunable physicochemical coding of material composition and topography in continuous microfibres. *Nat. Mater.* **2011**, *10*, 877–883.
- (19) Yu, Y.; Wen, H.; Ma, J.; Lykkemark, S.; Xu, H.; Qin, J. Flexible Fabrication of Biomimetic Bamboo-Like Hybrid Microfibers. *Adv. Mater.* **2014**, *26*, 2494–2499.
- (20) He, X.-H.; Wang, W.; Liu, Y.-M.; Jiang, M.-Y.; Wu, F.; Deng, K.; Liu, Z.; Ju, X.-J.; Xie, R.; Chu, L.-Y. Microfluidic Fabrication of Bio-Inspired Microfibers with Controllable Magnetic Spindle-Knots for 3D Assembly and Water Collection. *ACS Appl. Mater. Interfaces* **2015**, *7*, 17471–17481.
- (21) Ji, X. B.; Guo, S.; Zeng, C. F.; Wang, C. Q.; Zhang, L. X. Continuous generation of alginate microfibers with spindle-knots by using a simple microfluidic device. *RSC Adv.* **2015**, *5*, 2517–2522.
- (22) Shang, L.; Wang, Y.; Yu, Y.; Wang, J.; Zhao, Z.; Xu, H.; Zhao, Y. Bio-inspired stimuli-responsive graphene oxide fibers from microfluidics. *J. Mater. Chem. A* **2017**, *5*, 15026–15030.
- (23) Shang, L.; Fu, F.; Cheng, Y.; Yu, Y.; Wang, J.; Gu, Z.; Zhao, Y. Bioinspired Multifunctional Spindle-Knotted Microfibers from Microfluidics. *Small* **2017**, *13*, 1600286.
- (24) Peng, Q.; Shao, H.; Hu, X.; Zhang, Y. The Development of Fibers That Mimic the Core–Sheath and Spindle-Knot Morphology of Artificial Silk Using Microfluidic Devices. *Macromol. Mater. Eng.* **2017**, *302*, 1700102.
- (25) Tian, Y.; Zhu, P.; Tang, X.; Zhou, C.; Wang, J.; Kong, T.; Xu, M.; Wang, L. Large-scale water collection of bioinspired cavity-microfibers. *Nat. Commun.* **2017**, *8*, 1080.
- (26) Wu, Z.; Wang, J.; Zhao, Z.; Yu, Y.; Shang, L.; Zhao, Y. Microfluidic Generation of Bioinspired Spindle-knotted Graphene Microfibers for Oil Absorption. *ChemPhysChem* **2018**, *19*, 1990–1994.
- (27) Xie, R.; Xu, P.; Liu, Y.; Li, L.; Luo, G.; Ding, M.; Liang, Q. Necklace-Like Microfibers with Variable Knots and Perfusable Channels Fabricated by an Oil-Free Microfluidic Spinning Process. *Adv. Mater.* **2018**, *30*, 1705082.
- (28) Utada, A. S.; Lenceau, E.; Link, D. R.; Kaplan, P. D.; Stone, H. A.; Weitz, D. A. Monodisperse Double Emulsions Generated from a Microcapillary Device. *Science* **2005**, *308*, 537–541.
- (29) Hong, Y.; Wang, F. Flow rate effect on droplet control in a co-flowing microfluidic device. *Microfluid. Nanofluid.* **2007**, *3*, 341–346.
- (30) Zhu, P. A.; Wang, L. Q. Passive and active droplet generation with microfluidics: a review. *Lab Chip* **2017**, *17*, 34–75.
- (31) Mirri, G.; Škarabot, M.; Muševič, I. In situ laser-imprinted surface realignment of a nematic liquid crystal. *Soft Matter* **2015**, *11*, 3347–3353.
- (32) Yang, N.; Bruyn, J. R.; Hutter, J. L. Viscoelastic properties of poly(vinyl alcohol) nanofibers and hydrogels measured by atomic force microscopy. *Physics in Canada* **2008**, *64*, 141.
- (33) Humar, M.; Muševič, I. 3D microlasers from self-assembled cholesteric liquid-crystal microdroplets. *Opt. Express* **2010**, *18*, 26995–27003.